Development of improved blade tip endplate concepts for low-noise operation in industrial fans†

A Corsini[1*], **F Rispoli**[1], and **A G Sheard**[2]
[1]Dipartimento di Meccanica e Aeronautica, Sapienza University of Rome, Rome, Italy
[2]Fan Technology, Fläkt Woods Ltd, Axial Way, Colchester, Essex, UK

The manuscript was received on 1 November 2006 and was accepted after revision for publication on 13 April 2007.

DOI: 10.1243/09576509JPE386

Abstract: The application of improved blade tip geometries is studied with the aim of identifying an effective design concept for industrial fan passive noise control. The concept developed optimizes a datum blade by means of profiled endplates at the tip, reducing fan noise by changing the tip leakage flow behaviour. Experimental and computational investigations have been carried out on a family of axial fans, in fully ducted configuration, to establish the aerodynamic merits of the proposed blade tip design concept. The flow mechanisms in the fan tip region are correlated to specific blade design features that promote a reduction of the fan aero-acoustic signature in both tonal and broadband noise components. The tip vortical flow structures are characterized, and their role in creation of overall stage acoustic emissions clarified. The reported research identifies modification of tip geometry as markedly affecting the multiple vortex behaviour of blade tip leakage flow by altering the near-wall fluid flow paths on both blade surfaces. Blade tip endplates were also demonstrated to influence the rotor loss behaviour in the blade tip region. Improvement of rotor efficiency was correlated to the control of tip leakage flows.

Keywords: industrial fans, endplates, tip leakage flow, passive noise control

1 INTRODUCTION

Axial flow fan design specifications routinely demand large tip gaps in order to facilitate operation, first, in applications requiring a range of blade pitch angles and, second, in emergency smoke exhaust applications. The tip clearance flow is known to have detrimental affect on the rotor aero-dynamics [**1**–**3**], significantly contributing to the aero-acoustic signature of industrial axial flow fans used in the above-mentioned applications. The tip clearance flow is recognized as influencing the rotor noise spectra at discrete frequencies as a consequence of periodic velocity fluctuation associated with the tip flow vortex structure. Additionally, the broadband and high-frequency noise is influenced by velocity fluctuations in the blade passage [**4**–**7**].

As a consequence there is interest within both the academic and industrial community in looking for aerodynamic design methodologies that minimize negative effects of tip gap. By minimizing negative effect the aim is to manage blade tip to casing clearance flow structure that in turn minimizes impact of the flow structure on fan performance. Design methods and techniques that facilitate reduction of tip clearance noise without sacrificing aerodynamic efficiency have immediate application within a highly competitive industrial fan market.

The techniques for noise control in fans and compressors have been surveyed, and the solutions proposed grouped into two broad categories, active and passive noise control techniques. The two categories are conceptually designed to accomplish the goal of noise control by reducing the leakage flowrate or by

Corresponding author: Dipartimento di Meccanica e Aeronautica, Sapienza University of Rome, Via Eudossiana 18, Rome 100184, Italy. email: corsini@dma.ing.uniroma1.it

†*Extended version of a paper originally presented at the 2006 Conference on Modelling Fluid Flow (CMFF'06), Budapest University of Technology and Economics, 6–9 Sepetember 2006.*

enhancing the primary–secondary flow momentum transfer.

Active control techniques for fans and compressors reported in the literature consider the control of tip clearance flow by means of fluid injection on the casing wall in axial compressors [**8**] and low-speed axial flow fans [**9**]. Passive control techniques focus on, first, the exploitation of three-dimensional blade design techniques and, second, on modification of the blade and casing geometry in the gap region. The first approach makes use of sweep technique in blade design. This strategy is helpful in extending the aerodynamic limits of compressor and low-speed axial fan rotors by reducing secondary flows and in so doing positively affecting the rotor stall margin by unloading the blade tip [**10**–**12**].

The second family of control technique is based on manipulation of gap geometry, and makes use of casing treatments in the shroud portion over the blade tip. Opimization of shroud geometry was first identified in the early 1970s as a method by which the stable flow range of a compressor or fan could be extended by weakening the tip leakage vortex. Notable contributions focus on the use of grooves and slots [**13**, **14**] and stepped tip gaps [**15**]. Those scholars specifically interested in fan technology have proposed recirculating vanes and annular rings as antistall devices [**16**].

During the last decade a new technique for the control of noise in fans and compressors has been reported in the literature, advocating blade tip modifications by means of antivortex devices. This technique, already proven to represent good sealing configurations in pioneering works by Wadia and Booth [**17**, **18**], were first proposed in the noise control field by Quinlan and Bent [**6**], with ventilating fan patents proposing other solutions [**19**–**22**]. The research reported in this article aims to continue the development of antivortex devices, investigating the use of profiled endplates at the blade tip [**23**]. The study focuses on a family of commercially available industrial fans, and it reports on an experimental and numerical assessment of the aerodynamic and acoustic improvement in fan performance associated with application of optimized blade tip endplates.

The present study compares the aerodynamic and aeroacoustic performance of a datum blade with two other blades, each with improved but different tip geometries. The first blade has a tip endplate of constant thickness, whereas the second one is equipped with an endplate of variable profile thickness [**24**]. The experimental noise surveys were carried out in an anechoic chamber. The tip to casing flow field was modelled using a three-dimensional Reynolds-Averaged Navier–Stokes (RANS) solver. The authors adopt a parallel multi-grid scheme developed for the in-house finite element method (FEM) code [**25**]. The FEM formulation is based on a stabilized Petrov–Galerkin scheme developed for turbomachinery computational flow field analysis [**26**, **27**].

The numerical investigation facilitated insight into the tip leakage flow structure. The flow structure was analysed using, first, a vortical structure detection technique and, second, by identifying rotor loss behaviour. The assessment of benefit associated with the improved tip geometries is presented in terms of efficiency and gains in operating margin. The overall objective of the research is to investigate, via steady computational simulations, the technical merits of a passive control strategy for controlling the leakage flow and reducing tip clearance vortex/stator interaction noise and rotor tip self noise.

2 TEST AXIAL FLOW FANS

2.1 Test fans

The present study was performed on a family of commercially available industrial fans. In-service experiences indicated that this family of fans gives good acoustic performance with respect to present state-of-the-art fan technology for this type of application. The industrial fans studied have a six-blade unswept rotor, with blade profiles of modified ARA-D geometry, originally designed for propeller applications. The blade profile geometry is given for the datum fan AC90/6 at the hub and tip sections, respectively (Table 1).

The blade configurations studied for the datum and modified rotors feature a high tip stagger angle of 28°, measured, as is customary practice for industrial fan manufacturers, from the peripheral direction. This rotor angular setting has been chosen in order to exploit operating points where the vortical flow near the rotor tip dramatically affects the aerodynamic

Table 1 AC90/6 fan family specifications

	AC90/6 fans	
	Hub	Tip
Blade geometry		
ℓ/t	1.32	0.31
Stagger angle (°)	54	62
Camber angle (°)	46	41
Fan rotor		
Blade number	6	
Hub-to-casing diameter ratio ν	0.22	
Tip diameter (mm)	900.0	
Rotor tip clearance τ (% span)	1.0	
Rated rotational frequency (r/min)	900–935	

Blade profile geometry and rotor specifications.

performance and noise characteristics of the fans under investigation.

2.2 Fan tip endplates

The datum rotor and the improved rotors are referred to as AC90/6/TF and AC90/6/TFvte, with the thickness distributions of the improved tip concepts being compared with the datum blade (Fig. 1).

The improved blade tip geometry developed for the AC90/6/TF fan was inspired by a technique developed for tip vortex control and induced drag reduction. The technique suppresses unwanted three-dimensional flow features around aircraft wings, and has also been applied as an antivortex device on catamaran hulls.

The tip blade section was modified by adding an endplate along the blade pressure surface that ends on the blade trailing edge with a square tail. By introducing endplates, the blade section is locally thickened by 3:1 with respect to the maximum thickness at the tip of the datum blade. Endplate design theory indicates that an endplate thickness ratio of 3:1 is aerodynamically optimal, as the reference radial dimension of leakage vortex to be controlled is estimated to be in the range 0.2 to 0.1 per cent blade span, a figure favoured by those conducting early studies on the rotors of axial compressor [**28**] and fan [**12**].

A recent investigation, carried out by Corsini *et al.* [**23**], assessed the aerodynamics and aeroacoustics gains of rotor AC90/6/TF with respect to the datum rotor. The numerical simulation found evidence of a tip leakage vortex breakdown that affects the rotor AC90/6/TF at the design condition. This negative feature was found to be responsible for a loss in fan efficiency. Corsini and Sheard [**24**] eliminated the negative feature, identifying that the blade tip endplate should be designed such that the tip vortex flow was managed to control the vortex rotation number gradient below a critical safe value. The proposed blade tip geometry exploited a variable profile thickness distribution of the endplate and was named AC90/6/TFvte.

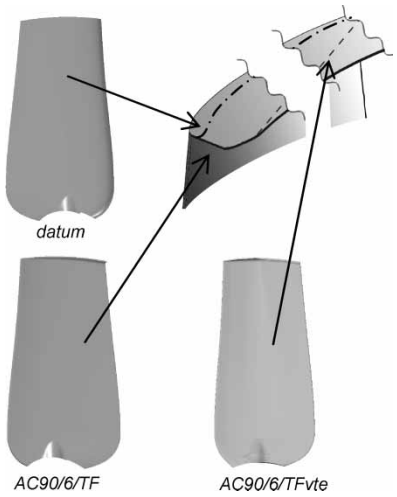

Fig. 1 Test fans and rotor blades (not to scale)

3 INVESTIGATION TECHNIQUES

The single rotor research was carried out at design operating conditions for three configurations of the studied six-blade axial flow fan, namely: the datum fan, coded AC90/6; and the two fans modified by the adoption of tip features, respectively, coded AC90/6/TF and AC90/6/TFvte. The experimental and numerical studies have been carried out in ducted configuration utilizing a high tip pitch angle of 28°, on the peripheral direction, for this angular setting the fan generates the highest static pressure and flowrate of its operational range.

The research compares datum, AC90/6/TF and AC90/6/TFvte fan rotors operated in near-design condition (D) with volume flowrate 7 m^3/s and global flow coefficient $\Phi = 0.278$. The Reynolds number based on tip diameter and rotor tip speed is 8.3×10^5, for ISO air condition.

3.1 Experimental procedure

The aerodynamic performance tests were conducted according to ISO 5801, for fully ducted configuration and installation type D. This installation features a ducted inlet and outlet, with an inlet bell mouth. The noise performance test was carried out in accordance with the British Standard BS848-2.6:2000, equivalent to ISO 10302:1996, employing a type A testing configuration. In this configuration the fan is placed downstream of a plenum chamber with a free outlet, an arrangement similar to that used for compact cooling fans.

3.2 Numerical procedure and axial fan modelling

The RANS equations are solved by an original parallel multi-grid finite-element flow solver [**25**]. Despite the steady-state simulation, the RANS is considered an effective investigation tool for vortical structure detection [**29**].

The physics involved in the fluid dynamics of incompressible three-dimensional turbulent flow-fields in the rotating frame of reference was modelled with a non-linear $k-\varepsilon$ turbulence model [**30**], here used in its topology-free low-Reynolds variant. This turbulence closure has been successfully validated on transitional compressor cascade flows, as well as high-pressure industrial fan rotors [**27**]. The numerical integration of partial differential equations (PDEs) is based on a consistent stabilized Petrov–Galerkin formulation

developed and applied to control the instability origins that affect the advective–diffusive incompressible flow limits, and the reaction of momentum and turbulent scale determining equations. The latter equations, respectively, related to the Coriolis acceleration and the dissipation/destruction terms in the turbulent scale determining equations [**26**]. Equal-order linear interpolation spaces are used for primary-turbulent and constrained variables, implicitly eliminating the undesirable pressure-checker boarding effects.

3.3 Axial fan modelling and boundary conditions

The mesh has been built according to a non-orthogonal body fitted coordinate system, by merging two structured H-type grid systems, the mesh in the main flow region, surrounding the blade, and an embedded mesh in the tip gap region. The mesh has $154 \times 68 \times 58$ nodes, respectively, in the axial, pitch, and span wise directions. In the axial direction the node distribution consists of 20, 50, and 30 per cent of nodes upstream of the leading edge, in the blade passage and downstream of it. There are 14 grid nodes to model the tip-clearance along the span (Fig. 2).

The mesh has an adequate stretch towards solid boundaries, with the ratio of minimum grid spacing on solid walls to midspan blade chord set as 2×10^{-3} on the blade tip, casing wall, and blade surfaces. The adopted grid refinement towards the solid surfaces controls the dimensionless distance δ^+ value about 1 on the first nodes row.

Standard boundary condition set has been adopted, already used in recent numerical studies on high performance fans [**11**, **12**].

The Dirichlet conditions for the relative velocity components are imposed at the inflow section half a midspan chord upstream the leading edge. The velocity profile has been obtained from flow simulation in an annular passage of identical hub-to-casing diameter ratio that includes an upstream spinner cone. The inlet distribution of the turbulent kinetic energy k is obtained from an axisymmetric turbulence intensity (TI) profile, derived on the basis of former studies on ducted industrial fans [**11**]. The TI profile features a nearly uniform value in the core region (about 6 per cent), growing markedly as the endwalls are approached (about 10 per cent). The inlet profile of turbulent kinetic energy dissipation rate is based on the characteristic length scale l_ε set to 0.01 of rotor pitch at midspan. Flow periodicity upstream and downstream the blading, and Neumann outflow conditions (homogeneous for k and ε and non-homogeneous for the static pressure) complete the set of boundary data.

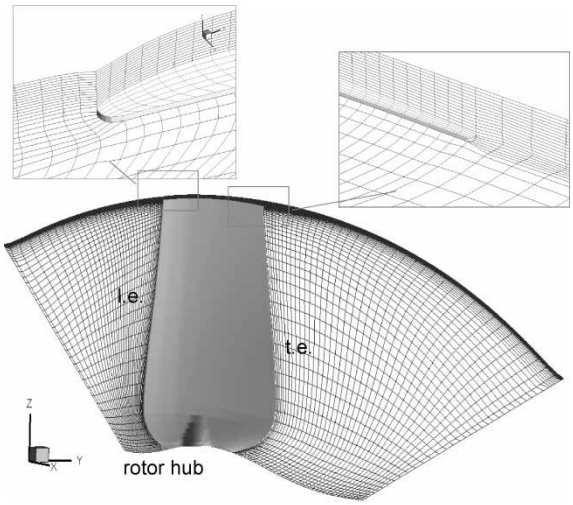

Fig. 2 Computational grid of fan rotor, mesh details in the tip gap region

4 PERFORMANCE EXPERIMENTS

4.1 Aerodynamic tests

The primary performance parameters measured were the fan static pressure and the efficiency. The static pressure and efficiency characteristic curves for datum, AC90/6/TF and AC90/6/TFvte rotors are compared (Fig. 3). Analysis of static pressure curves (Fig. 3)

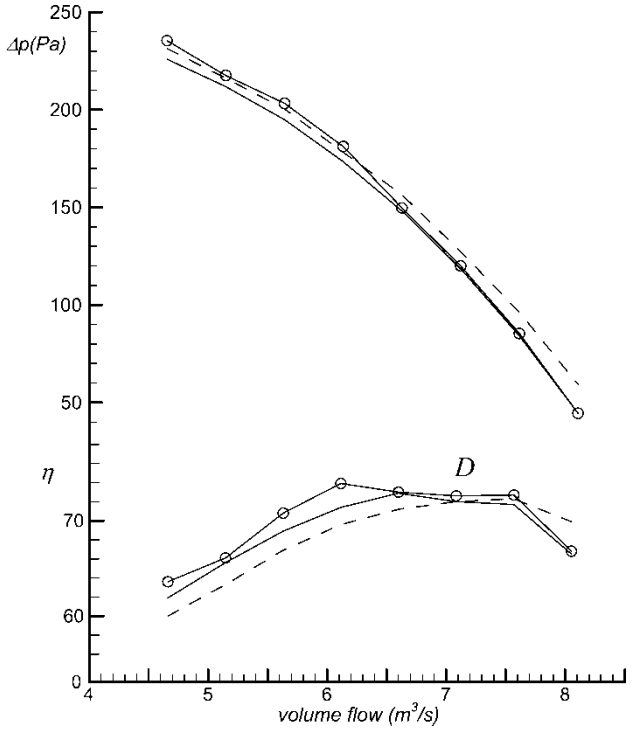

Fig. 3 Static pressure and efficiency characteristic curves (dashed lines: datum fan; solid lines: AC90/6/TF fan; line-symbols: AC90/6/TFvte fan)

Table 2 Predicted and measured fan overall performance at 7 m^3/s

	Measurements		Predictions	
	Δp_{stat} (Pa)	η	Δp_{stat} (Pa)	η
Datum	134.8	0.490	133.3	0.510
AC90/6/TF	126.2	0.510	126.1	0.504
AC90/6/TFvte	129.0	0.519	128.2	0.516

indicates a small performance reduction in rotor AC90/6/TF with improved tip concept of about 2 per cent at 6 m^3/s as a consequence of interaction between the tip clearance flow and the suction side near surface fluid [**31**]. This performance penalty is however partially recovered by rotor AC90/6/TFvte whose static pressure rise increases by throttling the rotor towards the peak pressure.

When the efficiency curves are studied, it becomes evident that both the modified rotors feature an efficiency improvement in the range of volume flowrate above the design volume flowrate. Moreover, the efficiency curve comparison indicates that the adoption of the tip endplates results in the appearance of a clear efficiency plateau, that shifts the peak η volume flowrate towards the rotor stall.

The rotor performance was assessed along the operating line. The predicted overall performance for 900 r/min rotational frequency are compared, Table 2, to the experimental data. Efficiency η is computed in terms of static pressure rise. The comparison confirms the validity of the predicted performance at the chosen blade angle, the blade angle at which the fan blades are most highly loaded and consequentially more prone to flow separation.

The prediction of performance parameters have been referred to axial sections, respectively, located at the inlet of the domain, and 20 per cent midspan chord downstream the blade trailing edge. The comparison validates the predicted performance.

4.2 Noise tests

The measured power spectra in one-third-octave band are compared (Figs 4(a) and (b)), for the measured sound power level and the A-weighted sound power level spectra. The noise tests have been conducted to compare the rotor aeroacoustic signature for identical static pressure rise, 190 Pa, close to each fan peak pressure operating point. Hemispherical acoustic measurements were performed at a radial distance from the fan outlet of 2 m, using ten locations of the probe.

Effectiveness of the improved tip concepts (Fig. 4) with constant and variable thickness endplates, is demonstrated by the reduction of the rotor aeroacoustic signature both in terms of tonal noise and broadband noise. These noise components are related to the main recognized tip noise generation mechanisms in axial decelerating turbomachinery. The convection of the primary tip vortex and its interaction with the statoric structures produces primarily tonal noise, while the oscillating tip vortex can be linked to the creation of broadband self-generated noise [**32**].

Figure 5 gives evidence of the noise reduction potential of the proposed original tip concepts by comparing the variation in the whole operating range of the unweighted overall sound power level (SWL), measured at a radial distance of 6 m from the fan outlet.

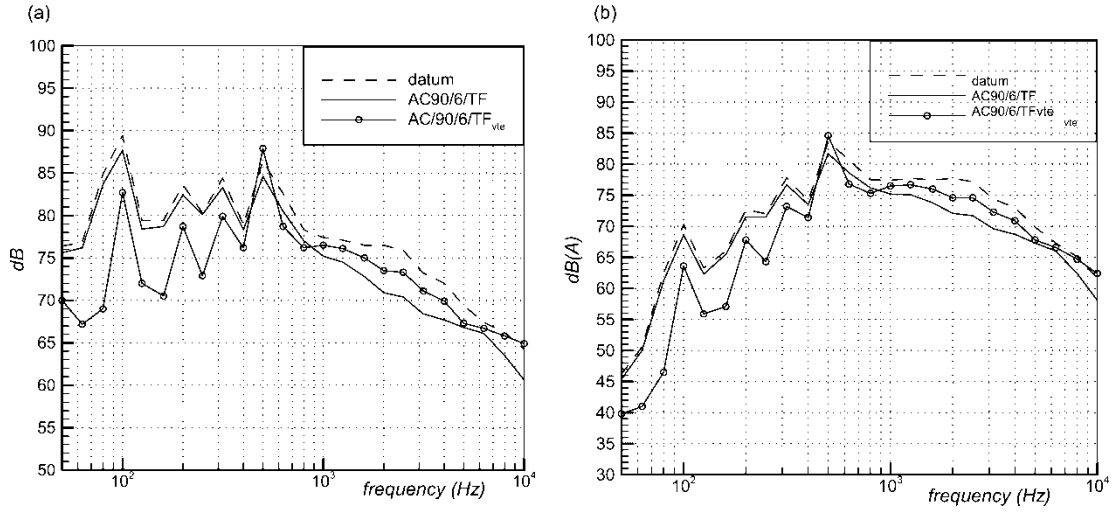

Fig. 4 Sound power level spectra in one-third-octave band. (a) Unweighted spectra and (b) A-weighted spectra (dashed lines: datum fan; solid lines: AC90/6/TF fan; line-symbols: AC90/6/TFvte fan)

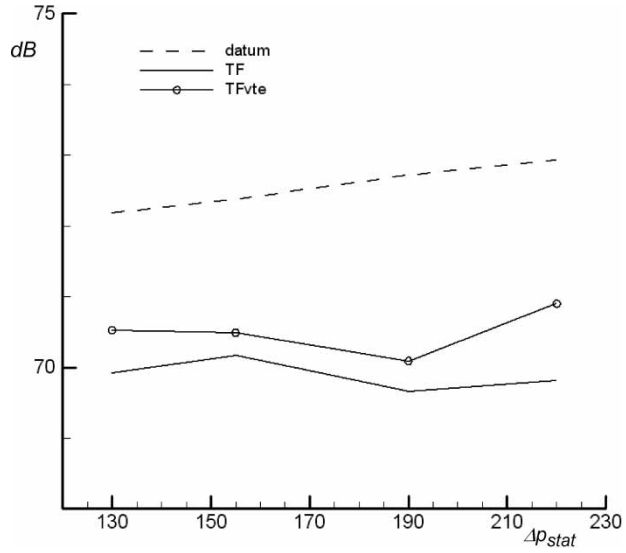

Fig. 5 Comparison of overall sound power level in the operating range (dashed lines: *datum* fan; solid lines; *TF* fan; line-symbols: *Tfvte* fan)

As evident, both the configurations markedly outperform the datum fan. It is also worth noting that the aerodynamic performance gain in AC90/6/TFvte fan is followed by a slight worsening of the acoustic signature in along the operating line.

5 INNER WORKINGS OF ENDPLATES

The improved blade tip concept, developed with use of constant and variable thickness endplates, has been demonstrated to reduce the aeroacoustic signature of the family of fans under investigations. This payoff appears in conjunction with an efficiency improvement in the peak pressure operating range.

The experimental data prompted a comparative investigation, against the datum fan, concerning the inner workings of the passive control device used to influence the structure of the tip leakage vortex and other systems of secondary vorticities. The effectiveness of the passive tip devices is analysed by comparing the normalized streamwise vorticity map evolution along the chord, and the tip vortex core paths. The analysis is complemented by the evaluation of tip leakage flow energy contents, affecting the rotor aeroacoustic signatures. The analysis is extended via the presentation of loss coefficient map evolution within the blade passage to assess influence of the modified geometry at the blade tip.

5.1 Helicity distributions and vortex cores

The tip leakage vortical structures are first investigated by using the normalized helicity H_n based on the absolute vorticity [**3**, **29**] as detection tool. H_n is defined and normalized as: $H_n = (\xi_i \cdot w_i)/(|\xi||w|)$ with $i = 1, \ldots, 3$, where ξ_i and w_i are the Cartesian components of the absolute vorticity and relative velocity vectors, $|\xi|$ and $|w|$ their norms. The normalized helicity distribution in the blade tip region is compared with the contours on cross flow planes in near-design operating condition (Fig. 6). The probing planes are located, respectively, at 0.25, 0.43, 0.65, 0.89, and 1.2 blade chord ℓ from the tip section leading edge. The normalized helicity distribution is plotted with the vortex cores coloured by the local magnitude.

For the fan rotors studied, a clear vortex core is only observed for the leakage flow structures emerging in the front portion of the tip blade sections. In the multiple vortex behaviour of datum fan rotor (Fig. 6(a)) the helicity field indicates that a main clockwise vortical structure (TLV1) develops through the passage with high skewing angle with respect to the blade surface.

The existence of a weak tip secondary vortex (Fig. 6(a)) corotating with TLV1, in the vicinity of the suction surface, can be identified on the 0.65ℓ plane by the streamwise vorticity distribution. In the front portion of the blade, 0.25ℓ downstream of the leading edge, the helicity map identifies the presence of a third vortical structure spreading from the leading edge of the blade. In the blade aft region, the leakage flow is mainly characterized by the merging of tip separation vortex TLV2 and leading edge vortex with TLV1 one, resulting in a unique clockwise vortical structure able to affect a large proportion of the blade pitch on the casing annulus.

There is evidence that the AC90/6/TF rotor tip flow is modified by the presence of the endplate (Fig. 6(b)). The existence of a vortex limiting the mass leakage along the blade pressure surface (Fig. 6(b)) constitutes evidence of the pressure side leg of a horse-shoe like structure. Similarly to the datum rotor, in the first quarter of the blade chord, the trace of an additional highly skewed leading edge vortex corotating with TLV1 is evident. Both the TLV1 and the leading edge vortices feature, since their appearance on the 0.25ℓ plane, a smaller in-passage extension coupled with a reduced helicity magnitude when compared to the datum rotor field. The leading edge vortex also never collapses into the TLV1, but decays as indicated on 0.43ℓ plane. Moving downstream, about midchord, the TLV1 features a gradual H_n reduction owing to the weakening of flow vorticity and to the deflection of the vortex core. This reduction agrees with the hypothesis of mass leaking reduction along the chord, that gives rise to a leakage flow structures nearly adjacent to the blade suction surface (i.e. TLV2 structure).

In the aft portion of the blade, due to the leakage flow unfeeding, the TLV1 collapses producing a bubble-type separation recognized as the evidence of a vortex breakdown by Corsini and Sheard [**24**]. The separated

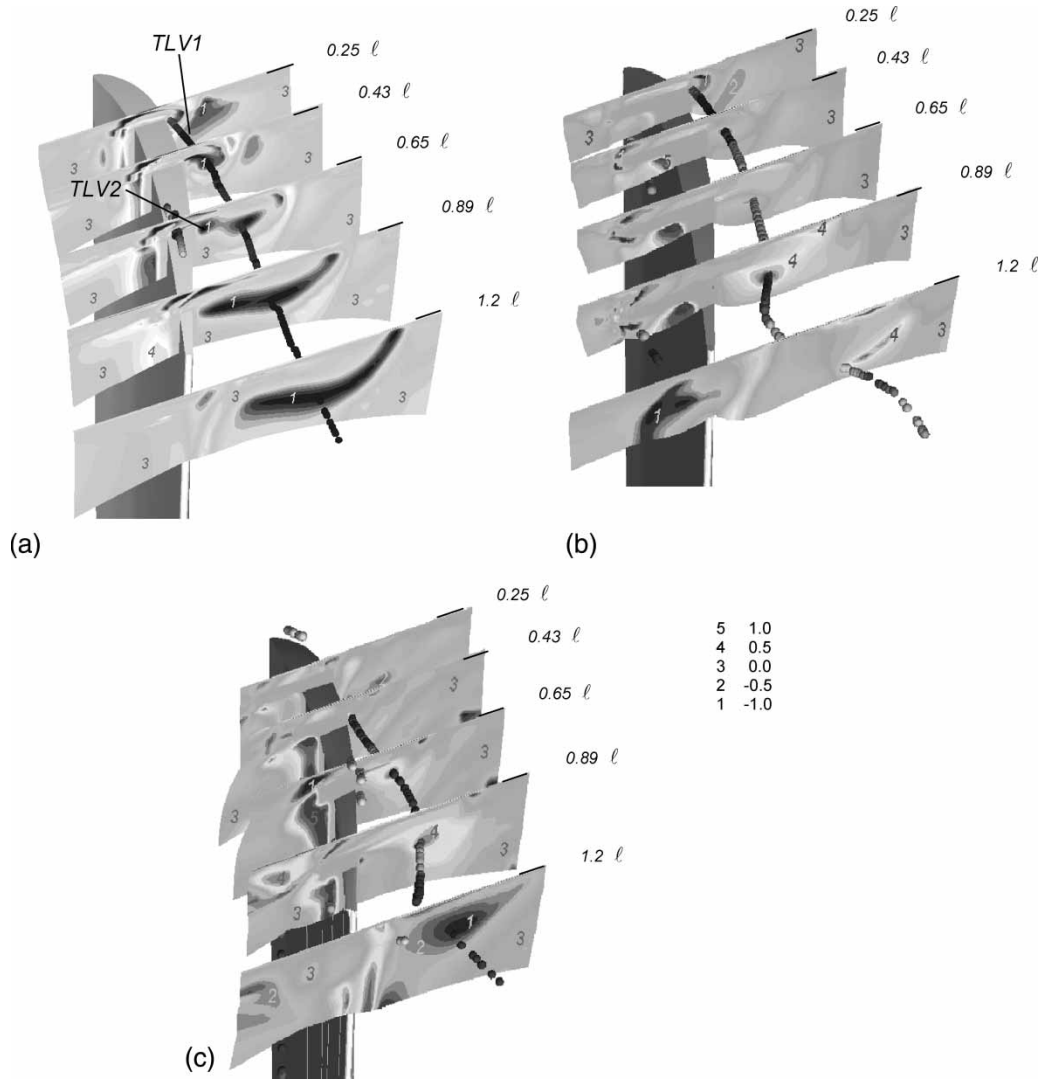

Fig. 6 Normalized helicity H_n contours on cross-sections and vortex cores at the tip, *D* operating point: (a) datum rotor, (b) AC90/6/TF rotor, and (c) AC90/6/TFvte

flow turns into a counter-clockwise vortex under the influence of trailing edge leakage flow streams, rapidly washing out the vortex behind the rotor so that on 1.2ℓ plane no coherent vortical structure is evident.

Finally, the use of the variable thickness endplate concept influences significantly the tip flow features (Fig. 6(c)). The onset of the main vortical structure *TLV1* moves downstream with respect to datum and AC90/6/TF blades, to about 0.3ℓ, and the vortex core path of TLV1 develops closer to the blade suction surface. At midchord, the weakened TLV1 vortex interacts with an anticlockwise rotating cell. This vortical core is lifted up from the pressure side boundary layer by highly energetic leakage jet and merges with TLV1 causing the inversion of its rotation. In the aft chord fraction, the tip vortex finally merges with a trailing edge rotating cell and exits the blade passage appearing as a coherent clockwise vortical structure. For this endplate configuration, the helicity maps confirms that a driving role is played by the pressure side

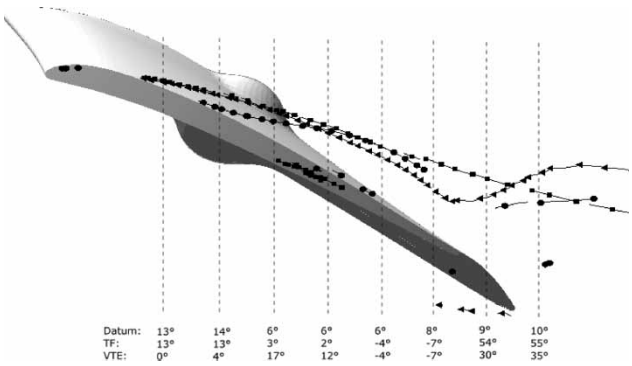

Fig. 7 Tip leakage vortex TLV1 trajectories (line-squares: datum, line-circles: AC90/6/TF; line-triangles: AC90/6/TFvte)

vortical structures as given by the horse-shoe vortex leg and by the corner vortex developing under the endplate.

The TLV1 vortex core trajectories are compared within the blade passage (Fig. 7) complemented by a chordwise comparison of leakage flow skewing angles. The vortex core path analysis gives further insight into the inner working of the developed endplates for leakage flow control.

Except for the location of vortex origins, both endplates feature TLV1 core trajectories developing along paths that are less skewed than the blade tip section. Because of the antivortex action exerted by the endplates, both the improved tip rotors feature a sudden deviation of TLV1 core behind the blade vane due to the interaction between the low energy leakage vortices and the passage flow.

5.2 Leakage flow energy

Investigation of leakage flow vortex energy contents completes the analysis of primary tip vortex structures. The rotational kinetic energy, defined on the basis of crosswise relative velocity components, and the resolved turbulent kinetic energy k are considered as benchmark quantities.

The sound sources, tonal in nature, are related to the energy contents of the tip leakage vortices moving in the axial direction and interacting with any stationary surfaces (primarily motor struts or outlet guide vanes). The rotational kinetic energy isolines within the tip gap at $R = 0.998$ are compared (Fig. 8) when the rotational energy is normalized by the bulk kinetic energy.

The datum rotor (Fig. 8(a)) features the highest rotational kinetic energy magnitude located at the onset of TLV1, where the leakage flow rolls up with energy content comparable to the reference one. The datum rotor map indicates evidence of a second highly rotating core tracing the tip separation vortex TLV2 previously observed (Fig. 6(a)). Both improved rotors (Figs 8(b) and (c)) therefore indicate that the endplates damp the leakage flow rotational kinetic energy utilizing two mechanisms. First, the reduction of the momentum transfer via leakage jet, at the TLV1 onset; second, as indicated by the rotational kinetic energy reducing by 50 per cent across the blade passage, the unfeeding of the leaked mass is able to further weaken the peripheral momentum transfer to tip vortices along the chord.

As a second energy marker the turbulent kinetic energy maps are studied by comparing the three-dimensional chordwise tip flow evolution on probing sections at 25, 43, 65, 89, and 120 per cent blade chord from the tip section leading edge. The k maps for the fans studied have been compared (Fig. 9) with the aid of simulated tip leakage stream-paths. The chordwise

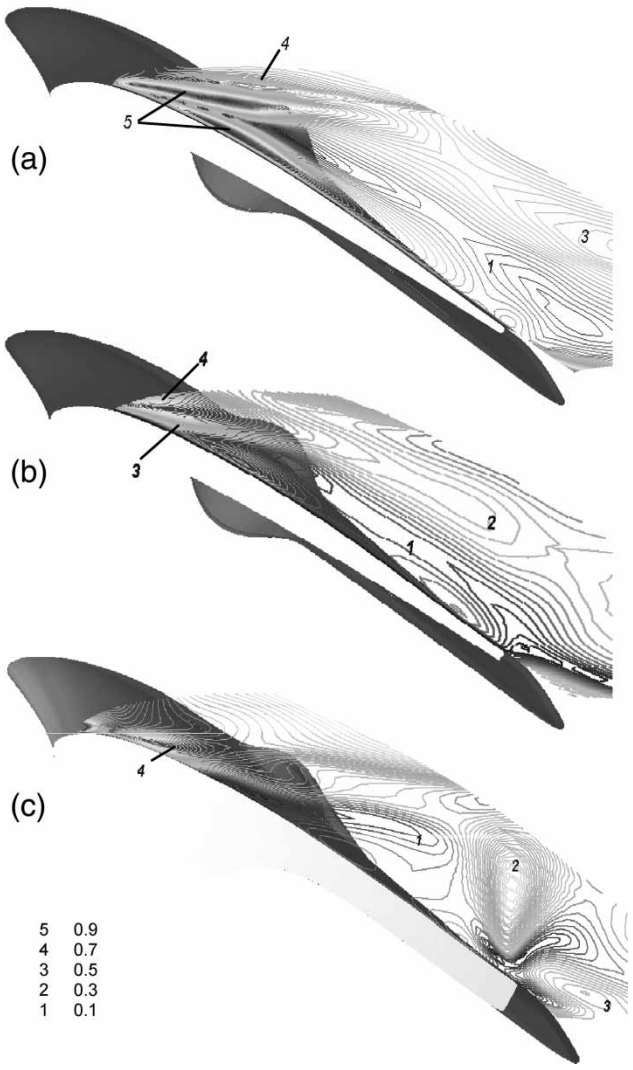

Fig. 8 Rotational kinetic energy isolines in the rotor tip gap at $R = 0.998$, D operating point: (a) datum rotor, (b) AC90/6/TF rotor, and (c) AC90/6/TFvte

evolution of turbulent kinetic energy maps (Fig. 9) indicates the significance of difference between the rotors under investigation, with the difference primarily concentrated in the vicinity of the casing annulus endwalls. As a general observation, in the presence of an antivortex device the attenuation of leakage flow results in an attenuation of the local turbulence level that reduces the peak turbulent kinetic energy within the leakage vortex cores. This is particularly evident (Figs 9(b) and (c)) where the primary tip vortex rolls up into a low turbulence level core. The peak k values remain concentrated in the interaction cores between the suction side near-surface fluid and the leakage flow. The AC90/6/TF rotor streamlines also confirm that the primary tip vortex collapses giving rise to a separation bubble structure, similar to the time-averaged evidence of leakage flow vortex breakdown (Fig. 9(b)) a phenomenon identified by Inoue

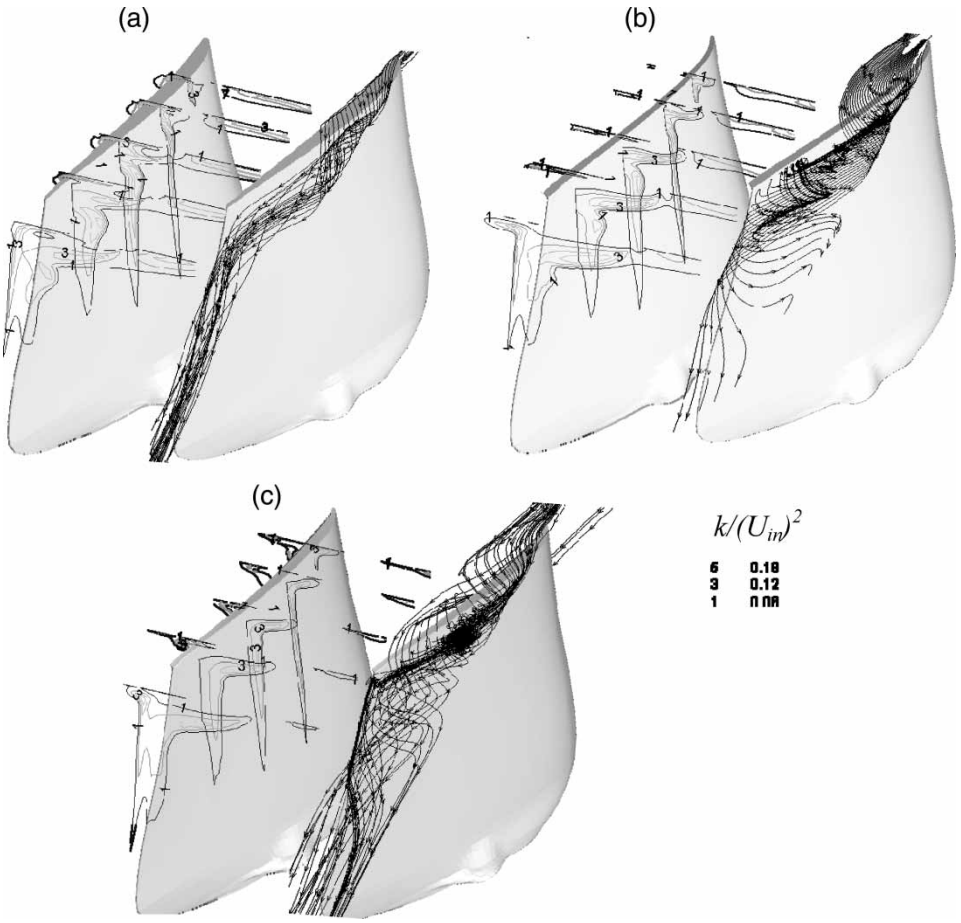

Fig. 9 Turbulent kinetic energy contours on cross-sections and tip vortex streamlines, *D* operating point: (a) datum rotor, (b) AC90/6/TF rotor, and (c) AC90/6/TFvte

and Furukawa [**29**]. It is evident (Fig. 9(c)) that the endplate variable thickness distribution is able to correct the TLV1 breakdown acting locally on the vortex rotation number on the basis of the endplate thickness distribution in the chord direction [**24**].

5.3 Loss at the rotor tip

Rotor loss behaviours at the blade tip are discussed with reference to the local total loss coefficient defined ζ. The loss behaviour is, finally, investigated with reference to the local total loss coefficient defined as: $\zeta = (\overline{p}_{0\text{in}} - p_0)/0.5\rho\overline{w}^2_{\text{in}}$, where p_0 is the local relative total pressure, $\overline{p}_{0\text{in}}$ and $0.5\rho\overline{w}^2_{\text{in}}$ are, respectively, the reference pitch-averaged relative total and dynamic pressures computed at the inlet midspan plane.

The total loss coefficient distribution within the blade passage (Fig. 10) is probing the flow fields in the vicinity of the blade leading edge, about midchord and in the region behind the blade (respectively, approximately 25, 65, and 120 per cent chord from the leading edge). The predicted loss evolutions (Figs 10(a) to (c)) in the design operating condition agree with the evidence found in literature for low-speed rotors and with the aerodynamic tests carried out. At the rotor inlet, all rotor distributions feature loss cores mainly concentrated on the hub annulus walls. Moving towards the blade aft, the loss maps are characterized by loss core directly related to the development of primary tip vortices travelling through the blade vane. A larger peak loss core affects the improved tip concept rotor AC90/6/TF (Fig. 10(b)) owing to the vortex breakdown. By comparing the AC90/6/TF and datum blade loss map on 1.2ℓ, it is evident that the improved tip rotor features a beneficial spanwise loss distribution, as it outperforms the datum fan within the wake and on the hub endwall where it gives healthier near wall layers on pressure and suction side corners.

When studying the AC90/6/TFvte fan rotor, there is evidence that the endplate design concept [**24**] functions (Fig. 10(c)). The leakage vortex breakdown is able to reduce the high loss core at the tip, behind the rotor and along the blade suction side within the interaction region between leakage and near-surface

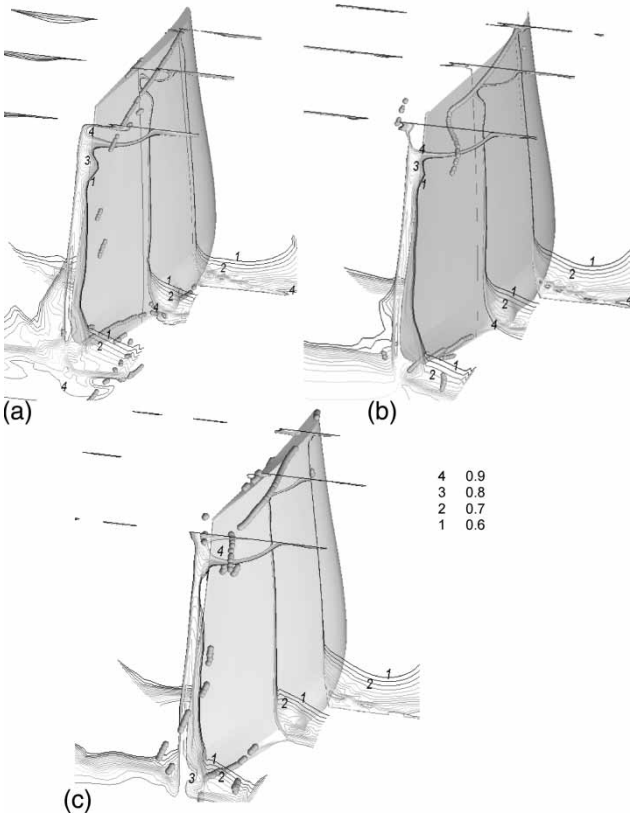

Fig. 10 Evolution of total pressure loss coefficient ζ inside the blade passage: (a) datum rotor, (b) AC90/6/TF rotor, and (c) AC90/6/TFvte

flows. This comparative behaviour, in agreement with the aerodynamic test results, is considered to be a consequence of the reduced three-dimensional flow rearrangement occurring as a consequence of the reduction in mass leaking through the tip gap. The limited radial migration of near-wall surface fluid induces smaller hub loss core and the contraction of suction/corner stall (Figs 10(b) and (c)).

6 CONCLUSIONS ON NOISE CONTROL BY ENDPLATES

Sound is a weak by-product of a subsonic turbulent flow, and noise generation control in fans is challenging because turbulence is relatively inefficient as an acoustic source. The analysis of leakage flow was intended to provide evidences of the aerodynamic mechanisms realized by the endplate based tip concepts for passive noise control. To this end, the phenomenological viewpoints, given in section 5, must be complemented by additional observations as to the influence endplates exert on the rotor aeroacoustics by altering the turbulent flow in the tip region.

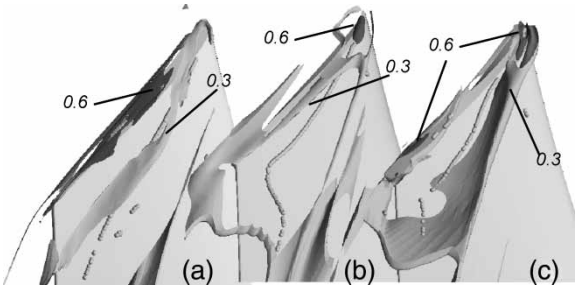

Fig. 11 Turbulence intensity iso-surfaces at the tip: (a) datum rotor, (b) AC90/6/TF rotor, and (c) AC90/6/TFvte

The endplates work as mixing enhancement devices, altering the turbulence statistics and the time- and length-scales of noise generating eddies. These modifications to the flow field directly impact on the sound field by modifying the low- and high-frequency noise components.

The effectiveness of tip endplates, AC90/6/TF and AC90/6/TFvte, is first discussed through a comparison of turbulence intensity TI iso-surfaces in the vicinity of the tip (Fig. 11) where two turbulence intensity levels have been taken, respectively, TI = 0.3 and TI = 0.6.

The datum rotor features a high turbulence level core concentrated about the tip blade (Fig. 11(a)) which develops over a significant fraction of the chord. The vortex core path entirely evolves within the conical iso-surface at TI = 0.3. With respect to this baseline, both the rotors exploiting the improved tip concepts share common features: the peak TI cores are located near the leading edge at the onset of the main leakage vortex (TLV1) and the vortex core trajectories remain inside low turbulence volumes bounded by the TI = 0.3 iso-surfaces, at the periphery of vortical regions that are remarkably larger than the in the datum rotor.

The turbulent viscosity (ν_t normalized by the molecular viscosity) distribution is compared in vicinity of the blade tip (Figs 12(a) to (c)) confirming that the improved tip rotors handle the leakage flow by

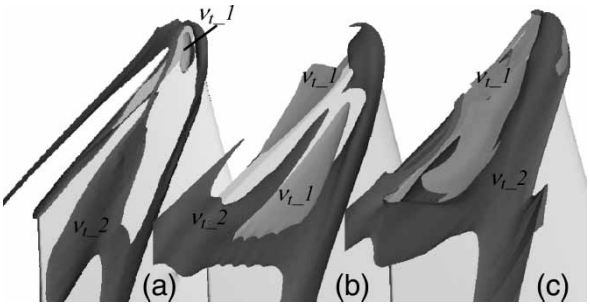

Fig. 12 Normalized turbulent viscosity ν_t iso-surfaces at the tip: (a) datum rotor, (b) AC90/6/TF rotor, and (c) AC90/6/Tfvte ($\nu_t 2{:}10^2\ \nu_{mol}$; $\nu_t 1{:}5 \times 10\ \nu_{mol}$)

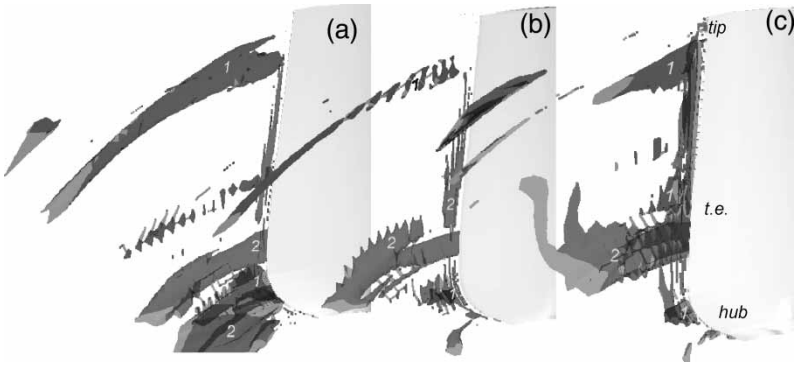

Fig. 13 Normalized helicity H_n iso-surfaces behind the fan rotors: (a) datum rotor, (b) AC90/6/TF rotor, and (c) AC90/6/TFvte (isosurface 1. $H_n = -1$, isosurface 2. $H_n = 1$)

enhancing the turbulent diffusion within the leakage vortices. The datum rotor features lower diffusion level in correspondence with the TLV1 path (Fig. 12(a)) and reach the peak viscosity level behind the blade where the vortex interacts with primary and secondary flows.

The subsonic broadband noise could be related to primary tip vortices that once formed are responsible for the convection of large-scale fluctuations downwind the trailing edge that are considered to gives rise to scattering and broadband noise [**32**]. Flow visualization and experimental measurements indicate that secondary flows overall the blade span contribute to the broadband noise generated by small cooling axial flow fans.

The normalized helicity distribution behind the rotors under investigation is compared (Fig. 13) to identify how the wake behaviour is affected by the adoption of endplates. It is concluded that the application of endplates extends beneficial effect from the tip region to the blade passage secondary flows (Figs 13(b) and (c)) with the helicity maps illustrating the reduction of secondary phenomena related to the wake and to the hub corner vortices.

7 SUMMARY

A study has been carried out, with the aim of identifying the structure of tip leakage flow and its influence on the fluid dynamical behaviour in a family of axial flow fans. The objective of the paper has been to investigate the effectiveness of improved blade tip concepts to control the leakage flow phenomena and rotor aeroacoustic signatures. Two endplate geometries have been developed the first one with constant thickness, and the second one with a variable thickness distribution according to a safe rotation number chordwise gradient concept.

The aerodynamic tests indicate that the improved tip concepts are affected by a small performance derating, but the measured efficiency indicates an improvement with increased peak performance and wider high efficiency plateau towards the rotor stall margin. The noise test demonstrated a reduction of the rotor aeroacoustic signature both in terms of tonal noise and broadband noise.

The investigation was based on an in-house developed parallel finite-element Navier–Stokes solver. The physical interpretation of the detailed three-dimensional flow field predictions were studied by means of streamlines, streamwise vorticity, or leakage flow kinetic energy, and loss maps.

The comparison of detected leakage vortical structure development indicated that the datum rotor features a multiple vortex behaviour characterized by a dominant leading edge vortical structure, highly skewed with respect to the local relative flow direction, and a weak tip secondary vortex in the vicinity of the suction surface. The presence of the endplates influence the leakage flows structure at the leading edge by changing its orientation with respect to the local relative streamlines that govern the secondary flow advection in the rotor frame. Both the rotors designed with the improved tip geometries appear to be characterized by two vortical structures at the tip, respectively, the trace of the pressure side leg of an incoming horse-shoe vortex like structure and the suction side trace of the main leakage flow. The existence of this pressure side vortex, peculiar of the improved tip concepts rotor, is recognized as one of the factor contributing to the control of the leakage phenomenon promoting a vena contracta effect. As a consequence the mass leaking is unfed close to the leading edge and the resulting control of leakage flow onset converts into potentially improved aeroacoustic performance.

The analysis of the leakage flow energy contents, indirectly related to the recognized tip leakage noise mechanisms, has provided evidence of a reduction in the rotational kinetic energy and turbulence level on the casing owing to the presence of the antivortex device.

The loss coefficient distributions confirm that the highest loss regions were always observed to coincidence with the leakage vortex core with a nearly constant peak loss value. The comparative analysis of mechanical energy loss within the tip gap showed that presence of the antivortex device at the tip leads to a reduction of mechanical energy loss within the gap, suggesting that the loss level within the tip gap is mainly controlled by the mass leaking.

ACKNOWLEDGEMENTS

The present research was done in the context of the contract FW-DMA07, between Fläkt Woods Ltd and Dipartimento di Meccanica e Aeronautica 'Sapienza' University of Rome. The authors gratefully acknowledge Mr I. Kinghorn and Mr B. Perugini for their contribution to the experiments.

REFERENCES

1 **Fukano, T.** and **Takamatsu, Y.** The effects of tip clearance on the noise of low-pressure axial and mixed flow fans. *J. Sound Vibr.*, 1986, **105**, 291–308.
2 **Storer, J. A.** and **Cumpsty, N. A.** Tip leakage flow in axial compressors. *J. Turbomach.*, 1991, **113**, 252–259.
3 **Furukawa, M., Inoue, M., Saiki, K.,** and **Yamada, K.** The role of the tip leakage vortex breakdown in compressor rotor aerodynamics. *J. Turbomach.*, 1999, **121**, 469–480.
4 **Fukano, T.** and **Jang, C.** Tip clearance noise of axial flow fans operating at design and off-design condition. *J. Sound Vibr.*, 2004, **275**, 1027–1050.
5 **Jang, C., Fukano, T.,** and **Furukawa, M.** Effects of the tip clearance on vortical flow and its relation to noise in an axial flow fan. *JSME Trans. B*, 2003, **46**, 356–365.
6 **Quinlan, D. A.** and **Bent, P. H.** High frequency noise generation in small axial flow fans. *J. Sound Vibr.*, 1998, **218**, 177–204.
7 **Vad, J., Koscso, G., Gutermuth, M., Kasza, Z., Tabi, T.,** and **Csorgo, T.** Study of the aero-acoustic and aerodynamic effects of soft coating upon airfoil. *JSME Trans. C*, 2006, **49**, 648–656.
8 **Bae, J. W., Breuer, K. S.,** and **Tan, C. S.** Active control of tip clearance flow in axial compressors. *J. Turbomach.*, 2005, **127**, 352–362.
9 **Roy, B., Chouhan, M.,** and **Kaundinya, K. V.** Experimental study of boundary layer control through tip injection on straight and swept compressor blades. ASME paper GT2005-68304, 2005.
10 **Wadia, A. R., Szucs, P. N.,** and **Crall, D. W.** Inner workings of aerodynamic sweep. *J. Turbomach.*, 1998, **120**, 671–682.
11 **Corsini, A.** and **Rispoli, F.** Using sweep to extend stall-free operational range in axial fan rotors. *Proc. Instn Mech. Engrs. Part A: J. Power and Energy*, 2004, **218**, 129–139.
12 **Corsini, A., Rispoli, F., Kinghorn, I. R.,** and **Sheard, A. G.** The aerodynamic interaction of tip leakage and mainstream flows in a fully-ducted axial fan. ASME paper GT2004-53408, 2004.
13 **Takata, H.** and **Tsukuda, Y.** Stall margin improvement by casing treatment – its mechanism and effectiveness. *J. Eng. Power*, 1977, **99**, 121–133.
14 **Smith, G. D. J.** and **Cumpsty, N. A.** Flow phenomena in compressor casing treatment. *J. Eng. Gas Turbines Power*, 1984, **106**, 532–541.
15 **Thompson, D. W., King, P. I.,** and **Rabe, D. C.** Experimental and computational investigation on stepped tip gap effects on the flowfield of a transonic axial-flow compressor rotor. *J. Turbomach.*, 1998, **120**, 477–486.
16 **Jensen, C. E.** *Axial-flow fan*. US Pat. 4,630,993, 1986.
17 **Wadia, A. R.** and **Booth, T. C.** Rotor-tip leakage: part II – design optimization through viscous analysis and experiment. *J. Eng. Power*, 1982, **104**, 162–169.
18 **Wadia, A. R.** Numerical calculations of time dependent three-dimensional viscous flows in a blade passage with tip clearance. AIAA paper 83-1171, 1983.
19 **Longet, C. M. L.** *Axial flow fan with noise reducing means*. US Pat. 2003/0123987 A1, 2003.
20 **Mimura, M.** *Axial flow fan*. US Pat. 6,648,598 B2, 2003.
21 **Belady, C. L.** *Winglet-enhanced fan*. US Pat. 6,776,578 B2, 2004.
22 **Uselton, R. B., Cook, L. J.,** and **Wright, T.** *Fan with reduced noise generation*. US Pat. 2005/0147496 A1, 2005.
23 **Corsini, A., Rispoli, F., Kinghorn, I. R.,** and **Sheard, A. G.** Investigation on improved blade tip concept. ASME paper GT2006-90592, 2006.
24 **Corsini, A.** and **Sheard, A. G.** Tip end-plate concept based on leakage vortex rotation number control. *J. Comput. Appl. Mech.*, 2007, accepted for publication.
25 **Borello, D., Corsini, A.,** and **Rispoli, F.** A finite element overlapping scheme for turbomachinery flows on parallel platforms. *Comput. Fluids*, 2003, **32**(7), 1017–1047.
26 **Corsini, A., Rispoli, F.,** and **Santoriello, A.** A new stabilized finite element method for advection–diffusion–reaction equations using quadratic elements. In *Modelling fluid flow* (Eds T. Lajos *et al.*), 2003, pp. 247–268 (Springer-Verlag, Berlin).
27 **Corsini, A.** and **Rispoli, F.** Flow analyses in a high-pressure axial ventilation fan with a non-linear eddy-viscosity closure. *Int. J. Heat Fluid Flow*, 2005, **26**, 349–361.
28 **Inoue, M., Kuroumaru, M.,** and **Furukawa, M.** Behavior of tip leakage flow behind an axial compressor rotor. *J. Gas Turbine Power*, 1986, **108**, 7–14.
29 **Inoue, M.** and **Furukawa, M.** Physics of tip clearance flow in turbomachinery. ASME paper FEDSM2002-31184, 2002.
30 **Craft, T. J., Launder, B. E.,** and **Suga, K.** Development and application of a cubic eddy-viscosity model of turbulence. *Int. J. Heat Fluid Flow*, 1996, **17**, 108–155.
31 **Gbadebo, S. A., Cumpsty, N. A.,** and **Hynes, T. P.** Interaction of tip clearance flow and three-dimensional separations in axial compressors. ASME paper GT2006-90071, 2006.
32 **Khourrami, M. R.** and **Choudari, M.** A novel approach for reducing rotor tip-clearance induced noise in turbofan engines. AIAA paper 2001-2148, 2001.

APPENDIX

Notation

D	design operating point
H_n	normalized helicity
k	turbulent kinetic energy
ℓ	chord length
l_ε	turbulence length scale
l.e.	leading edge
p	static pressure
P	peak-pressure operating point
PS	pressure side
r	radius
R	radial poistion normalized by tip radius
SS	suction side
SWL	sound power level
t.e.	trailing edge
TI	turbulence intensity
TLV	tip leakage vortex
U_c	casing relative peripheral velocity
v, w	absolute and relative velocities
x, y, z	Cartesian coordinates
γ	stagger angle
δ^+	normalized distance from the wall
ε	turbulent dissipation rate
ζ	total loss coefficient, $(\overline{p}_{0\text{in}} - p_0)/0.5\rho\overline{w}_{\text{in}}^2$
η	efficiency
ν	hub-to-casing diameter ratio
ν_t	turbulent viscosity
ξ_i	absolute vorticity vector
ξ_s	streamwise vorticity, $\xi_s = (\xi_i \cdot w_i)/(2\omega\|w\|)$
σ	blade solidity
Φ	global flow coefficient (annulus area-averaged axial velocity normalized by U_c)
χ	rotor tip clearance
Ψ	pressure rise coefficient $(\Delta p/(\rho 0.5 U_c^2))$
ω	rotor angular velocity

Subscripts and superscripts

a, p, r	axial, peripheral, and radial
c	casing wall
h	hub wall
i	Cartesian component index
in	inlet section
mol	molecular quantity
s	streamwise component
-	pitch-averaged value
0	total quantities